A comparative study of magnetic properties of $LiFePO_4$ and $LiMnPO_4$

2004 J. Phys.: Condens. Matter 16 5531

(http://iopscience.iop.org/0953-8984/16/30/014)

INSTITUTE OF PHYSICS PUBLISHING JOURNAL OF PHYSICS: CONDENSED MATTER

J. Phys.: Condens. Matter **16** (2004) 5531–5548 PII: S0953-8984(04)79785-4

A comparative study of magnetic properties of $LiFePO_4$ and $LiMnPO_4$

Denis Arčon[1,2], Andrej Zorko[1], Robert Dominko[3] and Zvonko Jagličić[4]

[1] Department of Solid State Physics, Institute Jožef Stefan, Jamova 39, 1000 Ljubljana, Slovenia
[2] Faculty of Mathematics and Physics, University of Ljubljana, Jadranska 19, 1000 Ljubljana, Slovenia
[3] National Institute of Chemistry, Hajdrihova 19, 1000 Ljubljana, Slovenia
[4] Institute of Mathematics, Physics and Mechanics, Jadranska 19, 1000 Ljubljana, Slovenia

Received 23 April 2004
Published 16 July 2004
Online at stacks.iop.org/JPhysCM/16/5531
doi:10.1088/0953-8984/16/30/014

Abstract

A detailed comparative study of the magnetic properties of $LiFePO_4$ and $LiMnPO_4$ samples is presented. Magnetic susceptibility, electron paramagnetic resonance and ^{7}Li NMR experiments were performed on samples as prepared for electrochemical studies. The ground state of $LiFePO_4$ seems to be that of a collinear antiferromagnet and very robust against crystal imperfections. On the other hand, our $LiMnPO_4$ samples possess a weak ferromagnetic ground state with a transition temperature $T_N = 42$ K. We suggest that solitons may be very important magnetic excitations in these systems and that pinning of solitons below T_N together with frustration plays a decisive role in the formation of the weak ferromagnetic state in $LiMnPO_4$. The differences between the magnetic properties of these two samples reflect also the differences between their electronic structures and may thus be important for the electrochemistry of $LiFePO_4$ and $LiMnPO_4$.

1. Introduction

Since the pioneering work of Goodenough *et al* [1], the phospho-olivines $LiMPO_4$ (where M stands for Fe, Mn, Co, Ni) have been recognized as a potential positive electrode material for use in lithium rechargeable batteries. This family of materials has numerous advantages over the layered rock salt oxides (e.g. $LiCoO_2$ and $LiNiO_2$) that are currently used in commercial batteries. Besides its high capacity ($\sim$170 mA h g^{-1}), $LiMPO_4$ cathode material shows high stability during lithium extraction/insertion and does not deteriorate when used at moderately high temperatures. Recently, a lot of effort has been devoted to optimization of $LiFePO_4$ material. In particular, particle minimization with intimate carbon contact resulted in almost the theoretical capacity at moderate current densities with $LiFePO_4$ cathode material [2].

Surprisingly, only few papers indicate the applicability of $LiMnPO_4$ [3–5] and, besides that, the results remain controversial.

The origin of the different electrochemical activities of isostructural $LiFePO_4$ and $LiMnPO_4$ is not quite clear at the moment. Yamada *et al* [3] suggested that the low electrochemical activity of $LiMnPO_4$ is due to slow kinetics and internal friction during lithium extraction/insertion. We have recently performed a comparative structural study [6] of these two materials and found minute differences in the oxygen vibrations in the Li layer. Yet another important factor is the magnetism in these compounds [7–9]. Magnetic properties are determined by the electronic states and may thus reflect the potential differences within the $LiMPO_4$ family. Magnetism is therefore indirectly important for the electrochemical properties as well.

In the olivine structure the magnetic ions occupy only the so-called M2 site, i.e. the M^{2+} ion sits in the centre of the MO_6 unit. Each MO_6 distorted octahedron is connected to four other MO_6 via vertices forming a layered network perpendicular to the crystal [100] axis. Successive M^{2+} layers are separated by PO_4 tetrahedra and LiO_6 octahedra.

Magnetic properties of $LiMPO_4$ were studied in the early 1960s. The magnetic structures of $LiCoPO_4$ and $LiNiPO_4$ are suggested to be those of collinear antiferromagnets [10] but they differ in the orientation of the sublattice magnetizations. In $LiCoPO_4$ the magnetic moments are oriented along the [010] direction while in $LiNiPO_4$ they point along the [001] direction. On the other hand, in $LiFePO_4$ the antiferromagnetic transition [10, 11] occurs at 52 K with magnetic moments aligned along the crystal [010] axis. And finally, $LiMnPO_4$ was again suggested to be a collinear antiferromagnet with a Néel temperature ranging between 35 K, for synthetic materials [8], and 42 K, for minerals [12].

However, with the discovery of the electrochemical activity of $LiFePO_4$ there has been a revival of interest in these materials. In this paper we revisit the magnetic properties of $LiFePO_4$ and $LiMnPO_4$ materials, as prepared for use as an active material for Li ion batteries. We emphasize that the focus of this study is on the magnetic properties of materials prepared for electrochemical studies with all possible defects, vacancies and particle size effects. In particular, we have performed SQUID magnetization, EPR and ^{7}Li NMR measurements between room temperature and 2 K. The measurements revealed differences in the magnetic ground states that could be important for the electrochemical activity of the $LiMPO_4$ family.

2. Experimental details

2.1. Sample synthesis

The samples were prepared by a standard sol–gel method [13]. As a starting precursor, iron (III) citrate (Aldrich, 22,897-4) or manganese (II) acetate tetrahydrate ($C_4H_6MnO_4 \times 4H_2O$, Fluka, 63537) and citric acid ($C_6H_8O_7 \times H_2O$, Kemika, 0319506) were dissolved at 60 °C in water. Separately, an equimolar water solution of LiH_2PO_4 was prepared from lithium phosphate (Li_3PO_4, Aldrich 33,889-3) and phosphoric (V) acid (H_3PO_4, Aldrich 31,027-1). Clear solutions were mixed together and dried at 60 °C for 24 h. After thorough grinding with a mortar and pestle, the xerogel obtained was fired in a reductive (5 wt% of hydrogen in argon) atmosphere at 700 °C ($LiFePO_4$) or 900 °C ($LiMnPO_4$) for 10 h. The powder obtained was black due to carbon-coated submicron particles (the content of carbon is about 6 wt%) [14]. The average size of coherent domains obtained from the analysis of the half-width of the x-ray diffraction peaks was, for both materials, in the range between 40 and 50 nm. The average particle size did not vary substantially from batch to batch. A typical active surface area was estimated to be around 60 $m^2\ g^{-1}$.

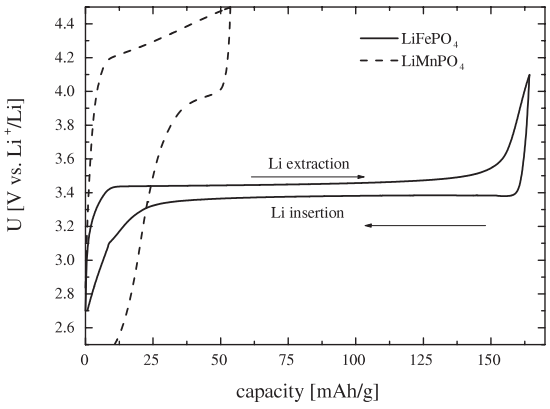

Figure 1. Lithium extraction/insertion in the second cycle at a current density of 8.5 mA g^{-1} (C/20 rate).

2.2. Electrochemical testing

The preparations of electrodes and systems for electrochemical testing are described elsewhere [15]. We should stress that the current density used for discharging/charging was set to a value of 8.5 mA g^{-1} (corresponding roughly to a C/20 rate). The cut-off voltages during the discharge and charge were 4.1 and 2.7 V for $LiFePO_4$ and 4.5 and 2.5 V versus the lithium metal reference for $LiMnPO_4$.

Typical charge and discharge curves for $LiFePO_4$ and $LiMnPO_4$ are shown in figure 1. Although the nominal capacities for the two materials are similar, the capacity obtained for $LiMnPO_4$ is three times lower than that for $LiFePO_4$ and, besides that, the large polarization of the $LiMnPO_4$ sample suggests hindered lithium extraction/insertion.

2.3. Magnetization and magnetic resonance measurements

The susceptibility and magnetization were measured with a Quantum Design SQUID magnetometer, equipped with a 5 T superconducting magnet.

Continuous wave (cw) EPR measurements were performed on a Bruker E580 spectrometer using a Varian dual resonator with a reference sample in the second resonator to account for the slight changes in the Q-factor during the measurements. In all the cw experiments a modulation field $H_{\mathrm{mod}} = 1$ G and $\nu_{\mathrm{mod}} = 100$ kHz were used. The temperature was stabilized within 0.2 K in a continuous flow cryostat, ESR 900. To estimate the EPR spin susceptibility, $Cu(SO_4)_2{\cdot}5H_2O$ has been used as a standard sample.

^{7}Li NMR measurements were performed at a Larmor frequency $\nu_{\mathrm{L}} = 104.9$ MHz in a superconducting magnet, at 6.3 T. The ^{7}Li NMR spectra were, over the entire temperature range, broader than the measurement window determined with the 90° rf pulse width 6 μs. The spectra were therefore measured via the intensity of the echo signal while sweeping the resonance frequency in steps of 10 kHz. We also used automatic tuning of the resonance circuit in the frequency range between 103.5 and 106 MHz. The spin–lattice relaxation time T_1 was measured using a saturation–recovery technique with appropriate phase cycling.

3. Results

3.1. Magnetic susceptibility measurements

In figure 2 we show the temperature dependence of the static spin susceptibility in $LiMnPO_4$ powder. We stress that we found in this particular sample traces of Li_3PO_4 impurities. In

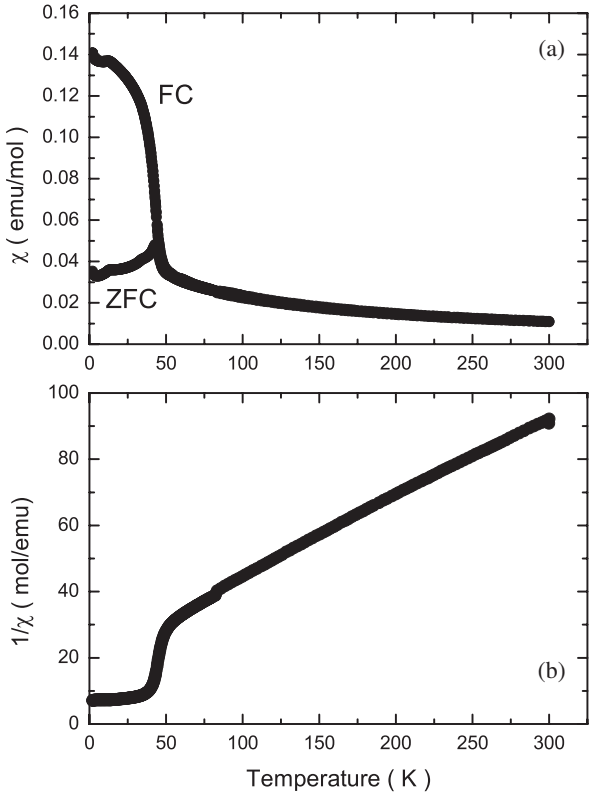

Figure 2. The temperature dependence of the (a) spin susceptibility and (b) inverse spin susceptibility for $LiMnPO_4$ powder. Please note the difference between the field cooled (FC) and zero-field cooled (ZFC) experiments.

an independent check, we tried to examine the magnetic properties of Li_3PO_4 using EPR but failed to find any paramagnetic signal. We therefore conclude that the Li_3PO_4 impurities cannot contribute to the total spin susceptibility presented in figure 2. At high temperatures, i.e. at temperatures between room temperature and 50 K, we observe a Curie–Weiss behaviour with a Curie constant $C = 4.23(1)$ emu K mol^{-1} and a Curie–Weiss temperature $\Theta = -87(2)$ K. These constants do not vary significantly from sample to sample. The susceptibility also shows the same behaviour between room temperature and ∼40 K, irrespective of the cooling protocol. However, around 40 K we observe an anomaly which is strongly dependent on whether the sample has been cooled in zero field or in a magnetic field. While in zero-field cooled experiments we observe a cusp in the magnetic susceptibility at $T_N = 39$–42 K, in field cooled experiments the susceptibility suddenly increases below T_N and then at lower temperatures saturates. The same type of behaviour can also be seen from the temperature dependence of the inverse susceptibility (figure 2(b)) where $1/\chi$ suddenly decreases at T_N. We stress that the magnitude of the saturated moment slightly varies from sample to sample. However, it will be shown later with ^{7}Li NMR measurements that this is still an intrinsic phenomenon and not a result from some unknown impurity phase.

Further evidence for the magnetic ordering comes from the ac susceptibility measurements, which clearly show a peak at T_N. We would like to stress that the peak position is frequency independent, i.e. it is precisely the same at $\nu = 1$ Hz as at $\nu = 100$ Hz, excluding the possibility of some spin-glass or superparamagnetic-like behaviour.

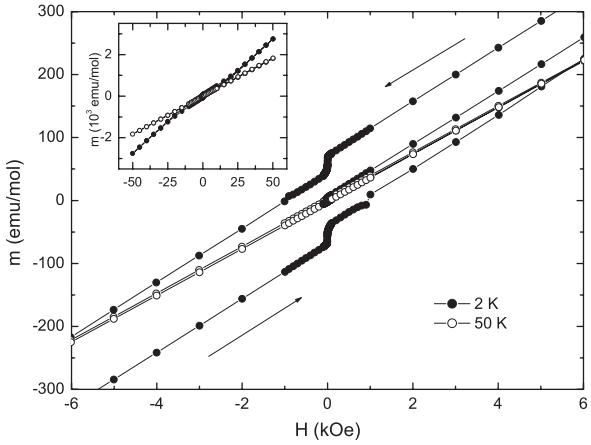

Figure 3. Magnetization curves measured for powdered $LiMnPO_4$ at 50 K (open circles) and at 2 K (solid circles). The measurements are displayed only for fields between −6 and 6 kOe, while complete magnetization versus magnetic field cycles are shown in the inset. The arrows indicate the direction of the change of the magnetic field.

Finally, we show in figure 3 hysteresis curves measured for a $LiMnPO_4$ powder sample. One can clearly see the hysteresis in the 2 K curve. The coercive field is about 1000 Oe, while the remanent magnetization is about 70 emu mol^{-1}. This remanent magnetization corresponds to 0.012 μ_B/Mn. Interestingly, we find a structure in the hysteresis just around zero field. The hysteresis disappears at $T = 50$ K, i.e. at temperatures above T_N. At this temperature we measure only a straight paramagnetic line.

The magnetic susceptibility of $LiFePO_4$ is less complicated (figure 4). Again, at high temperatures the magnetic susceptibility follows a Curie–Wess behaviour with a Curie constant $C = 4.28$ emu K mol^{-1} and a Curie–Weiss temperature $\Theta = -115(1)$ K. The susceptibility clearly shows a maximum characteristic of antiferromagnetic ordering at 50 K. No noticeable difference between zero-field cooled and field cooled experiments has been found. On the basis of these experiments, we can conclude that $LiFePO_4$ goes into a collinear antiferromagnetic ground state below $T_N = 51(1)$ K.

3.2. EPR measurements

The EPR line in $LiMnPO_4$ has a Lorentzian lineshape over the entire temperature range. This result is somewhat surprising as typically for a 2D lattice formed by the Mn ions one would expect deviations from the Lorentzian lineshape as a result of the spin diffusion processes. The EPR peak-to-peak linewidth is, at room temperature, 298 G. We note that this linewidth is larger by an order of magnitude than the one measured for perovskite layered Mn square-lattice antiferromagnets [16].

The temperature dependence of the EPR signal intensity, which is, in the paramagnetic phase, directly proportional to the static spin susceptibility, is shown in figure 5(a). At room temperature the intensity of the line corresponds to the spin susceptibility $\chi_{EPR} = 1.05 \times 10^{-2}$ emu mol^{-1}, which is nearly the same as the one measured by the SQUID (figure 2). This proves that we detect all Mn spins in these EPR measurements. At high temperatures the intensity of the signal follows the one measured by the SQUID magnetometer. The temperature dependence of the EPR spin susceptibility can be fitted with a Curie–Weiss law:

$$\chi_{EPR} = \frac{C}{T - \Theta}, \tag{1}$$

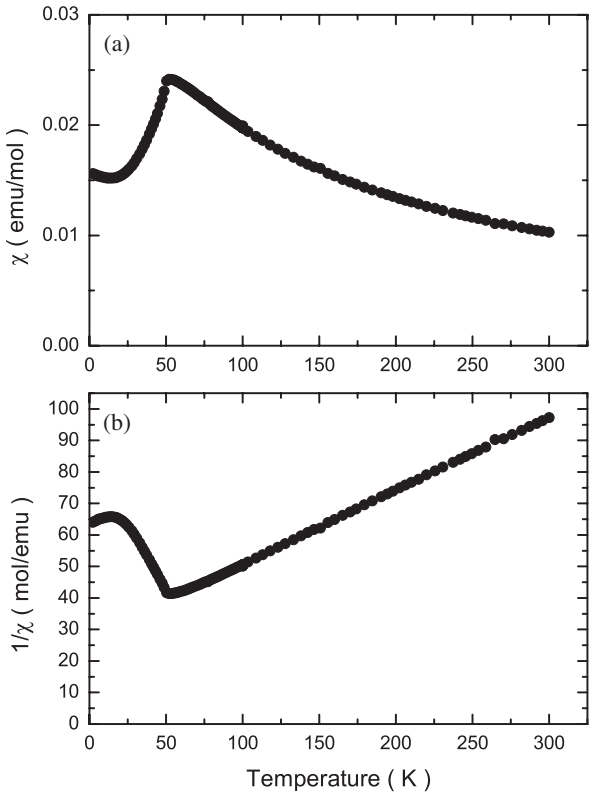

Figure 4. The temperature dependence of the (a) spin susceptibility and (b) inverse spin susceptibility for $LiFePO_4$ powder.

where $C = 3.92(2)$ emu K mol^{-1} is the Curie constant and $\Theta = -105(2)$ K is the Curie–Weiss temperature. We note that the extracted Curie–Weiss temperature is slightly more negative than the one obtained from SQUID measurements.

On cooling below around 45 K the EPR signal starts to disappear quite rapidly; it nearly vanishes in an interval of a few kelvins and almost completely vanishes at 42 K. This proves that the magnetic transition observed in SQUID measurements is indeed intrinsic and is not related to some unidentified impurities. We were not able to detect antiferromagnetic resonance in powdered $LiMnPO_4$ below T_N. We have however been able to measure the residual EPR signal down to 4 K. The origin of this signal will be discussed later.

Although the centre of the line (i.e. the g-factor) is nearly temperature independent (figure 5(b)), the linewidth exhibits a pronounced temperature dependence (figure 5(c)). In the entire temperature interval between room temperature and T_N the linewidth increases monotonically with decreasing temperature. At T_N the linewidth nearly diverges. In figure 6 we show the temperature dependence of the EPR linewidth on two different scales: $\ln \Delta H$ versus $(T - T_N)/T_N$ and $\ln(\Delta H - \Delta H(\infty))$ versus J/T. In the first graph we are testing the power-law behaviour while in the second one we are looking for an activated type of behaviour of the EPR linewidth. An attempt to fit the temperature dependence of the EPR linewidth to the power-law behaviour

$$\Delta H(T) = \Delta H_0 + \Delta H_0^P \left(\frac{T - T_N}{T_N} \right)^{-\beta} \tag{2}$$

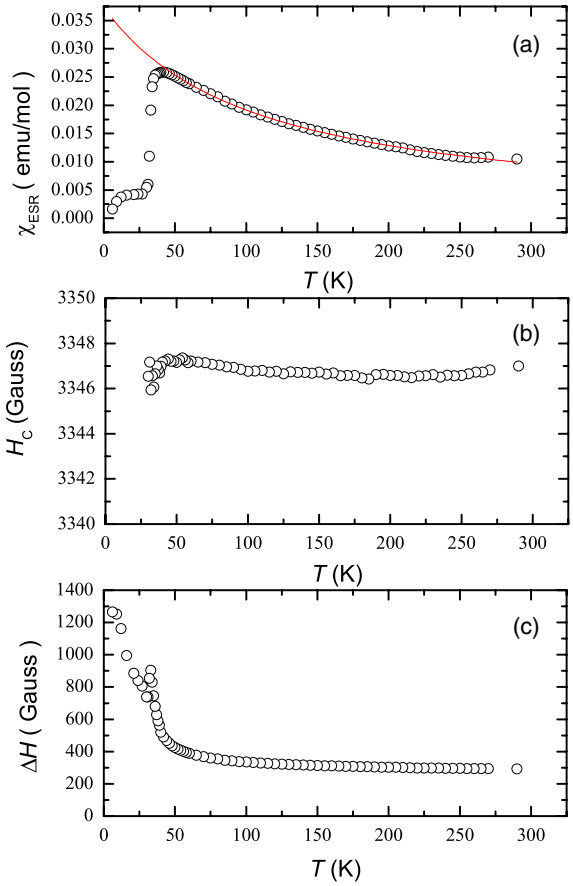

Figure 5. The temperature dependence of the (a) intensity, (b) centre and (c) linewidth of the Lorentzian EPR signal for $LiMnPO_4$ powder.

(This figure is in colour only in the electronic version)

is shown in figure 6(a). The parameters used in the fit are the linewidth at infinite temperature $\Delta H_0 = 236(2)$ G, $\Delta H_0^P = 134(3)$ G and the power exponent $\beta = 0.45(1)$. Surprisingly, this fit successfully describes the temperature dependence of the linewidth over a wide temperature interval, although it is difficult to believe that the critical fluctuations would survive even at temperatures as high as 10 T_N!

On the other hand, we notice that one can describe the temperature dependence of the EPR linewidth in the paramagnetic phase also with an activated type behaviour $\Delta H \propto \exp(E_a/T)$ where $E_a = 120$ K (see the dotted curve in figure 6(b)). In that case the deviation of the temperature dependence of the EPR linewidth from the activated type of behaviour just above the T_N reflects the critical fluctuations. The data were thus fitted with a sum of two contributions, i.e. the activated type contribution and the power-law contribution

$$\Delta H(T) = \Delta H_0 + \Delta H_0^a \exp(E_a/T) + \Delta H_0^P \left(\frac{T - T_N}{T_N}\right)^{-\beta}. \quad (3)$$

An unconstrained fit (the solid curve in figure 6(b)) led to the activation energy $E_a = 144(3)$ K and power exponent $\beta = 0.38(6)$. A deviation at higher temperatures (i.e. at lower J/T values)

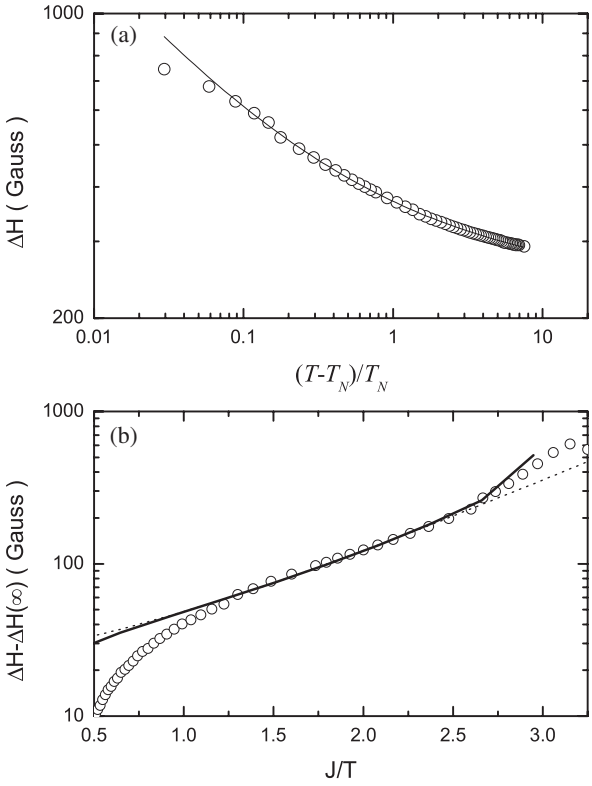

Figure 6. The temperature dependence of the EPR linewidth for $LiMnPO_4$ powder in (a) a 'power-law' graph and (b) an 'activation-law' graph.

can also be a signature of the spin diffusion contribution to the EPR linewidth, which makes ΔH_0 weakly temperature dependent. The possible origin of the activated type behaviour of the EPR linewidth will be discussed later.

Finally, we would like to mention that we were not able to detect the X-band EPR signal for $LiFePO_4$, most probably due to the extreme linewidth of the signal.

3.3. ^{7}Li NMR spectra

In figure 7 we compare the temperature dependences of the ^{7}Li NMR signals measured for $LiMnPO_4$ and $LiFePO_4$. We stress that the linewidth exceeds our excitation window even at room temperature and that we were thus forced to measure the spectra by sweeping the resonance frequency. We also note that the lineshape does not simply correspond to quadrupole broadened powder spectra. The lineshape has a shoulder on the high frequency side of the spectrum and can be satisfactorily fitted to the lineshape expected for a uniaxial shift tensor interaction. This would suggest that we are in fact observing only a central $-\frac{1}{2} \leftrightarrow \frac{1}{2}$ transition broadened due to a coupling to electronic spins residing at the metal sites. The satellite transitions may be smeared out over the whole frequency range and they are very difficult to detect in powder samples. We also note that the shift from the Larmor frequency is rather small, suggesting that the contact hyperfine coupling constants are rather small for these compounds. This result is in agreement with recent high temperature ^{7}Li MAS NMR results [23].

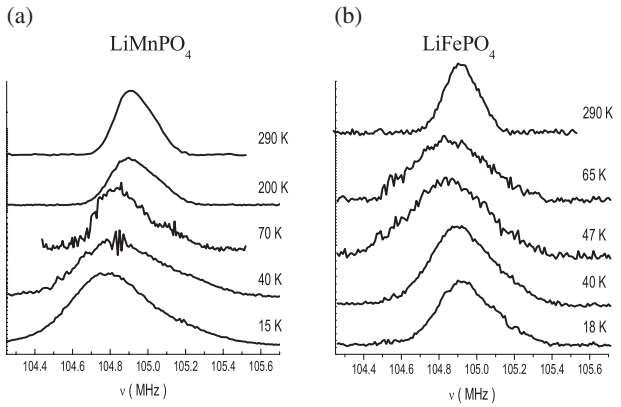

Figure 7. The temperature dependence of the ^{7}Li NMR signal for (a) $LiMnPO_4$ and (b) $LiFePO_4$ powder.

On cooling, the ^{7}Li NMR line is shifted to lower resonance frequencies and continuously broadens for both samples. This reflects the Curie–Weiss temperature dependence of the magnetic susceptibility. However, below the Néel temperature the two samples behave qualitatively differently. While for the $LiMnPO_4$ sample the linewidth tends to increase even below T_N, for $LiFePO_4$ the line narrows. This difference indicates that different local fields are experienced by the ^{7}Li nuclei below T_N in the particular two samples studied. The results clearly suggest that in $LiFePO_4$ the magnetic ordering is indeed antiferromagnetic. This is seen from the fact that the local field at the ^{7}Li site decreases below the transition temperature. On the other hand, in $LiMnPO_4$ the magnetic ordering is weak ferromagnetic type as evidenced by the broadening of the ^{7}Li NMR spectra. Possible origins of the weak ferromagnetism in our $LiMnPO_4$ sample will be discussed later.

The changes in the lineshape can also be seen in the temperature dependence of the moments of the ^{7}Li NMR spectra (figure 8). The temperature dependence of $\sqrt{M_2}$, which is approximately a measure of the linewidth of the spectra, on cooling steadily increases for both samples (figure 8(a)). For instance, $\sqrt{M_2}$ increases from 82 kHz at room temperature to around 200 kHz at 60 K. However, below the Néel temperatures again the two samples behave qualitatively differently. $\sqrt{M_2}$ for $LiMnPO_4$ suddenly increases below 40 K and then nearly saturates at the value of 350 kHz. On the other hand, for $LiFePO_4$ the second moment below 50 K starts to decrease and, for instance, at 15 K it amounts to only $\sqrt{M_2} \sim 135$ kHz. The same observations seem to hold for the first moments as well (figure 8(b)). For both samples the line first paramagnetically shifts on cooling. However, at T_N the line continues to shift for $LiMnPO_4$ while for $LiFePO_4$ the shift of the ^{7}Li NMR line reverses its trend.

So, to summarize this section, the local fields experienced by the ^{7}Li NMR probe on cooling from room temperature at first increase as expected for a paramagnetic phase. However, below T_N the two samples are qualitatively different. In $LiFePO_4$ the local field decreases while in $LiMnPO_4$ the local field increases below T_N. This suggests that the ground state of the sample of $LiFePO_4$ studied is indeed antiferromagnetic, but that of $LiMnPO_4$ is weak ferromagnetic.

3.4. ^{7}Li relaxation

Spin dynamics is reflected in the spin–spin relaxation time T_2 and spin–lattice relaxation time T_1. The spin–spin relaxation time has been measured in two different ways: first by

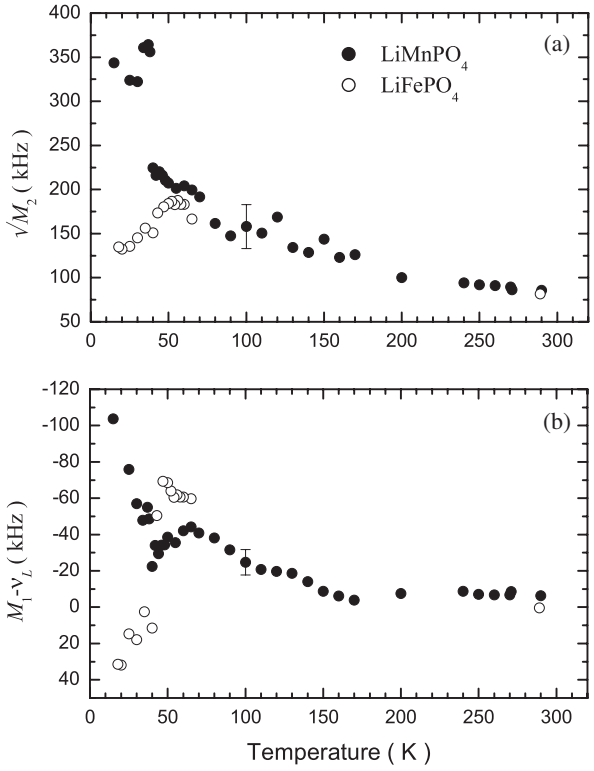

Figure 8. The temperature dependences of the (a) second-moment and (b) the first-moment ^{7}Li NMR spectra of $LiMnPO_4$ (solid circles) and $LiFePO_4$ (open circles).

monitoring the decay of the Hahn echo as a function of the separation time τ between the two pulses and second by means of the Carr–Purcell–Meiboom–Gill (CPMG) sequence [24]. Typical relaxation curves measured for $LiMnPO_4$ are shown in figure 9. The magnetization curve obtained from the decay of the Hahn echo is clearly non-exponential. A non-exponential decay is usually a signature of diffusion processes and has a characteristic time dependence:

$$E_{\mathrm{HE}}(\tau) = E_0 \exp\left(-\frac{2\tau}{T_2} - \frac{2}{3}(\gamma G)^2 D\tau^3\right). \tag{4}$$

Here T_2 is the decay rate of transverse magnetization in a uniform field, τ is the time interval between the two pulses in the Hahn-echo experiment, γ is the nuclear gyromagnetic ratio, $G = \partial B/\partial z$ is the gradient of the magnetic field, which is assumed to be uniform, and D is the appropriate self-diffusion coefficient. In many cases one wishes to determine the diffusion constant by intentionally applying a field gradient. However, even if the external magnetic field is homogeneous, local inhomogeneity in the spin susceptibility may take over and effectively lead to a very similar behaviour. In such a case one would expect to find $G = \frac{\partial \chi}{\partial z} B$, which could thus be relevant in the paramagnetic systems.

To avoid the extra decay due to diffusion, the Carr–Purcell–Meiboom–Gill (CPMG) sequence is often used. The experiments (a typical example is shown on figure 9(b)) were performed using different times τ between 180° pulses. The data obtained were then analysed using a simple exponential form $E(\tau) = E_0 \exp\left(-\frac{2\tau}{T_2}\right)$. We note however that the extracted spin–spin relaxation time T_2 depends on the value of τ used in the CPMG sequence. A typical

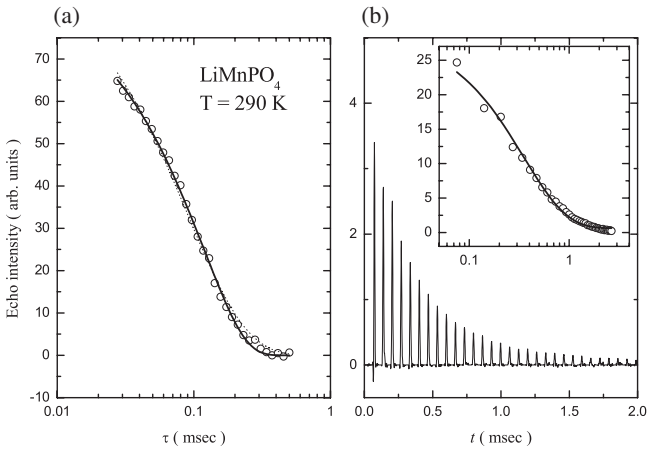

Figure 9. The decay of the echo intensity in $LiMnPO_4$ as a function of τ in (a) a simple Hahn-echo experiment and (b) a Carr–Purcell–Meiboom–Gill (CPMG) experiment. In the inset we show the decay of the echo in the CPMG experiment. The temperature is 296 K here.

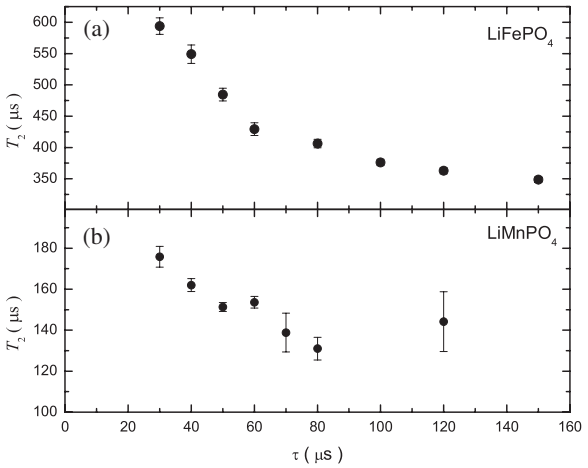

Figure 10. The dependence of the relaxation parameter T_2 obtained from the CPMG measurements for (a) $LiFePO_4$ and (b) $LiMnPO_4$ at $T = 290$ K.

example of such a dependence is shown in figure 10. For very small values of τ, i.e. when $\tau = 30\ \mu$s, the extracted parameter T_2 approaches the values obtained from a two-pulse Hahn-echo experiment. For larger values of $\tau > 50\ \mu$s, the extracted parameter T_2 on the other hand becomes smaller by almost a factor of two. The effect is much more pronounced for $LiFePO_4$, indicating that the slow motions responsible for the τ dependence of the parameter T_2 are more active on the timescale of $\tau \sim 30$–$50\ \mu$s.

In figure 11 we show the temperature dependence of the spin–spin relaxation time as obtained from the CPMG sequence with $\tau = 30\ \mu$s for both samples. Interestingly, the relaxation time is, around room temperature, more or less temperature independent and, for instance, for $LiFePO_4$ amounts to $590 \pm 25\ \mu$s, while for $LiMnPO_4$ it is slightly smaller and corresponds to $180 \pm 35\ \mu$s. On cooling however, T_2 exhibits anomalous behaviour. For instance, for $LiFePO_4$, about 10 K above the transition temperature, T_2 starts to get smaller,

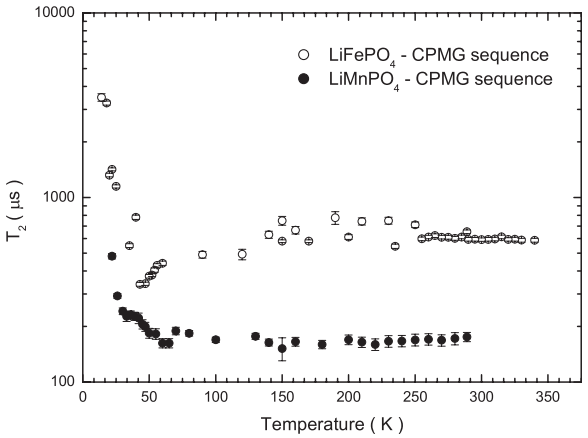

Figure 11. The temperature dependence of the spin–spin relaxation time T_2 obtained with the two-pulse Hahn-echo method and the CPMG method (here $\tau = 30\ \mu$s).

i.e. the relaxation rate T_2^{-1} becomes enhanced. At 47 K we thus have $T_2 = 340 \pm 12\ \mu$s, which is smaller by a factor of 1.7 than the room temperature value. Below the antiferromagnetic transition temperature, T_2 starts to rapidly increase with decreasing temperature and reaches 3.49 ± 0.05 ms at 12 K. Such behaviour signals the antiferromagnetic critical fluctuations just above the transition temperature and then, in the magnetically ordered phase, a slowing down of the electron spin dynamics as expected. Interestingly we do not find clear evidence for critical behaviour of $LiMnPO_4$, but below the Néel temperature the spin–spin relaxation time increases again.

We have also measured the spin–lattice relaxation time using a saturation–recovery method. The relaxation curves were found to be of the stretched exponential form

$$M_Z(t) = M_0(1 - r\exp(-(t/T_1)^{\alpha})) \tag{5}$$

over the entire temperature range. This suggests that the dominant relaxation mechanism is the fluctuation of the hyperfine coupling to the Mn^{2+} magnetic moments. Furthermore, we also note that the spin–lattice relaxation times T_1 obtained are very small—over most of the temperature range, of the order of 1–2 μs, again requiring electron–nuclear hyperfine coupling. In figure 12 we show the temperature dependence of the parameter T_1. The stretched exponential factor α was found to be very weakly temperature dependent. We see that the parameter T_1 is more or less temperature independent between room temperature and 60–70 K and, for instance, for $LiMnPO_4$ corresponds to about 1.5 ms. Just above the transition temperature the spin–lattice relaxation rate $1/T_1$ becomes enhanced (figure 12). Such an enhancement of the relaxation rate signals a critical slowing down of the magnetic fluctuations, as we have seen in T_2 measurements. This effect is again more obvious for $LiFePO_4$ than $LiMnPO_4$. Below T_N the spin–lattice relaxation time T_1 suddenly starts to increase (see the inset to figure 12), signalling the freezing out of the electronic spin dynamics. We also note that the parameter α is for $LiMnPO_4$ about 0.85 ± 0.1 and for $LiFePO_4$ is about 0.96 ± 0.05. Such stretched exponential forms of the magnetization relaxation curves are often found in systems exhibiting frustration and/or local disorder. A simple conclusion would thus be that the local disorder and frustration play more important roles for $LiMnPO_4$ than for $LiFePO_4$.

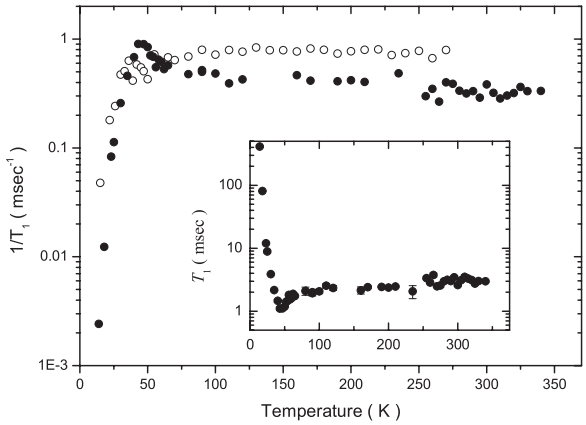

Figure 12. The temperature dependence of the spin–lattice relaxation rate $1/T_1$ for $LiMnPO_4$ (open circles) and $LiFePO_4$ (solid circles). In the inset we show the temperature dependence of the spin–lattice relaxation time T_1 for $LiFePO_4$.

4. Discussion

The structures of $LiMnPO_4$ and $LiFePO_4$ are isomorphous. They both crystallize in the olivine type crystal structure with orthogonal space group $Pnma$. The profile refinement by the FULLPROF program gives for $LiMnPO_4$ the room temperature lattice constants $a = 10.4447(6)$ Å, $b = 6.1018(3)$ Å, $c = 4.7431(3)$ Å [6]. The Mn–Mn distance is shortest in the b–c plane, at 3.92 Å. The Mn–Mn distance is much longer in the perpendicular direction, along the crystal a-lattice, i.e. 5.62 Å. These parameters suggest a quasi-two-dimensional character for the magnetic properties of $LiMnPO_4$. However, the Mn–O–Mn bonding is rather complicated and the Mn lattice cannot be simply treated as a two-dimensional square lattice. This is clearly reflected in the temperature dependence of the magnetic susceptibility, which can be, in the paramagnetic phase, simply fitted with a Curie–Weiss law (equation (1)). An unconstrained fit of the temperature dependence of the $LiMnPO_4$ susceptibility leads to a Curie temperature $\Theta = -87 \pm 2$ K and a Curie constant $C = 4.23(1)$ emu K mol^{-1}. The Curie constant obtained corresponds to the effective magnetic moment $\mu_{\text{eff}} = 5.82(2)\ \mu_{\text{B}}$, which is close to but slightly less than the value expected for Mn(II) spins ($S = 5/2$).

A similar observation holds also for $LiFePO_4$, where the susceptibility again follows a Curie–Weiss law between room temperature and 60 K with a Curie constant $C = 4.28(2)$ emu K mol^{-1} and a Curie–Weiss temperature $\Theta = -115(1)$ K. In this case the Curie constant corresponds to the effective moment $\mu_{\text{eff}} = 5.85(4)\ \mu_{\text{B}}$, which is in agreement with the Fe^{2+} high spin $S = 5/2$ state. We note that the temperature dependence of the susceptibility does not follow the dependence predicted for the 2D square lattice of classical spins [17] as it does not show a typical broad maximum. The sign of the Curie temperature for both samples suggests predominantly antiferromagnetic coupling between the spins.

We stress once again that we obtained, in EPR measurements, a spin-only susceptibility for about 15% higher Curie temperatures (see section 3.2). One can use a classical result to estimate the exchange coupling constant:

$$J = \frac{3k_{\text{B}}\Theta}{2zS(S+1)} \tag{6}$$

where z is the number of nearest neighbours. The estimated exchange coupling constant is $J_{\text{ex}} = 2.5$ K for $LiMnPO_4$, while for $LiFePO_4$ it is $J_{\text{ex}} = 3.3$ K.

The low temperature magnetic ground states of the $LiMnPO_4$ and $LiFePO_4$ samples studied in this work are not quite the same. While $LiFePO_4$ does indeed order into a collinear antiferromagnetic ground state as reported [10, 11], this is not the case for $LiMnPO_4$. Our $LiMnPO_4$ seems to order into a weak ferromagnetic ground state. This seems to be in contrast to the collinear antiferromagnetic state reported earlier for bulk samples [8]. The weak magnetic moment is thus associated with the particle sizes and morphologies. We remind the reader once again that our samples were primarily prepared for electrochemical studies, as mentioned above. Possible reasons for the occurrence of weak ferromagnetism in our $LiMnPO_4$ samples will be discussed below. The fact that the very small saturation magnetization varies from sample to sample could suggest that the magnetization is connected to some extrinsic impurities. However, careful structural investigations and EPR measurements seem to rule out this possibility and prove that this is indeed an intrinsic effect. Furthermore, the ^{7}Li NMR results unambiguously prove that, first, the sample is homogeneous (i.e. we do not find evidence for two kinds of Li sites) and, second, the size of the local magnetic field experienced by Li increases below T_N and does not decrease as expected for a collinear antiferromagnet and as was indeed observed for $LiFePO_4$. At the heart of this behaviour could be finite particle size effects. Finite particle size effects may have some impact on the magnetic properties of the samples studied in this work. That is, it is known that the magnetic behaviour of a particle surface differs from that corresponding to the bulk because of the different atomic coordination, compositional concentration and nature of the defects. The results of the magnetic resonance studies are consistent with enhancement of the magnetic anisotropy of the $LiMnPO_4$ sample. Consequently, finite size effects could be responsible for the change of the magnetic ground state from collinear antiferromagnetic to weak ferromagnetic.

The magnitude of the spontaneous magnetization in $LiMnPO_4$ and the fact that it is dependent on the cooling procedure also suggests that the frustration in $LiMnPO_4$ may be more important than in $LiFePO_4$. In order to shed some additional light on this problem, we now try to connect the bulk susceptibility measurements with the magnetic resonance data. The spin dynamics is reflected in the temperature dependence of the EPR linewidth. The power-law analysis shown in figure 6 manages to fit the data rather well. We note that the exponent $\beta = 0.45$ is an acceptable value for the Heisenberg antiferromagnetic system. However, we find it somewhat difficult to accept that the critical behaviour would survive even at temperatures $T > 5T_N$. Other mechanisms which could play an important role in the temperature dependence of the EPR linewidth usually result in different temperature dependences, i.e. in decrease of the EPR linewidth with decreasing temperature. For instance, one can consider spin diffusion decay of the spin correlation function, but this mechanism leads to linearly temperature dependent behaviour [18]. Another possibility is to consider the effect of static spin correlations on the linewidth. In principle this could be observed in low dimensional magnetic systems up to temperatures of the order of $T \sim 10$ J, but again it predicts narrowing of the EPR line with decreasing temperature [19]. Still another possibility arises if significant spin–phonon coupling which modifies the magnetic anisotropy interaction is present in the system. In this case one expects the linewidth to be directly proportional to the temperature; i.e. it would decrease with decreasing temperature [20]. So, all of these models predict decrease of the EPR linewidth with decreasing temperature, which has not been observed here. It is possible though that such behaviour would be observed at high temperatures. On the other hand, we prove in figure 6 that the data can be, over a rather broad temperature interval, fitted to some activated type of behaviour. In this plot the critical fluctuations are observed only extremely close to the magnetic transition. An activated type of behaviour can of course have many different origins. We stress however that for the layered perovskites such a behaviour has been interpreted in terms of nonlinear soliton excitations [16].

The soliton energy of the Belavin–Polyakov solution [21] is given by the expression

$$E_S = 4\pi J_{ex} S^2. \tag{7}$$

Taking the previously estimated value for the exchange energy $J_{ex} = 2.5$ K, one can calculate the soliton energy to be $E_S = 195$ K. Given the crudeness of the estimation of the exchange energy, we find this to be a rather satisfactory agreement with the experimentally determined activation energy $E_a = 144$ K. We note however that the introduction of a very small amount of impurity into the magnetic sites of a classical two-dimensional antiferromagnet leads to there being a new type of static (impurity-pinned) soliton that drastically affects the parameter E_a measured from the linewidth of the EPR signal [22]. It may well be that in our case the defects act as pinning centres for solitons. Therefore, one may suggest that in the low temperature magnetic phase of $LiMnPO_4$ a significant number of solitons are frozen around impurity centres. The residual EPR signal could thus originate from such centres.

A closer look at the ^{7}Li NMR data seems to support the above physical picture of $LiMnPO_4$. In paramagnetic systems of quadrupolar nuclei the electron–nuclear interaction (both contact as well as dipolar) is strong enough to influence not only the relaxation time but also the powder lineshape. The principal axis of the anisotropic electron–nuclear interaction does not necessary coincide with the unique axis of the electric field gradient tensor. This then introduces additional orientational dependent broadening of the ^{7}Li NMR lineshape and a very complex asymmetric ^{7}Li lineshape.

According to very recent ^{7}Li MAS NMR study of $LiMPO_4$ (M = Mn, Fe) these paramagnetic materials contain a single type of Li site in agreement with the olivine structure [23]. The isotropic shifts fall outside the known chemical shift range for Li in diamagnetic compounds and seem to suggest a significant electron–nuclear coupling. We note however that hyperfine coupling of the ^{7}Li nucleus to unpaired metal d electrons can result only from transfer of unpaired spin density via the oxygen p orbitals to the Li s orbitals. In such a case we expect the first moment of the line to follow the spin susceptibility measured by the SQUID. It has also been noted that such transfer of spin density can occur along two different 'paths', i.e. through the four 'right-angle' bonds with a Li–O–Fe angle of 95°–97° and four 'bent' bonds with a Li–O–Fe angle of 110°–122°.

In view of this, the appropriate spin Hamiltonian for the particular ^{7}Li nuclei would be

$$\mathcal{H} = \mathcal{H}_Z + \mathcal{H}_{en} + \mathcal{H}_Q. \tag{8}$$

Here, the first term

$$\mathcal{H}_Z = -\gamma \vec{I} \cdot (\mathbf{1} - \sigma) \cdot \vec{B}_0 \tag{9}$$

is the Zeeman term with the chemical shift σ already included. Typical values for the chemical shift of the Li nuclei in diamagnetic systems are about 20 ppm. Here we expect that, due to the character of the Li–O bond and increasing covalency of the ligands, the anisotropy of the chemical shift tensor will be even smaller [25]. The chemical shift anisotropy will thus be neglected in the forthcoming analysis. The second term is the term describing the coupling of the Li nucleus to the electronic spins $\mathcal{H}_{en}$. This coupling is then further composed from the dipolar interaction between the Li nuclei and the unpaired metal magnetic moments, as well as from the contact interaction due to a partial transfer of unpaired spin density to the Li s orbital:

$$\mathcal{H}_{en} = \sum_i A^i_{iso} \langle \vec{S}^i \rangle \cdot \vec{I} + \sum_k \langle \vec{S}^k \rangle \cdot \mathbf{T}^k \cdot \vec{I}. \tag{10}$$

Here the sum over i runs over all Fe (Mn)–O–Li bonds. With the brackets $\langle\,\rangle$ we also reflect the fact that the dynamics of the electronic spins is, on the NMR timescale, so fast that one has

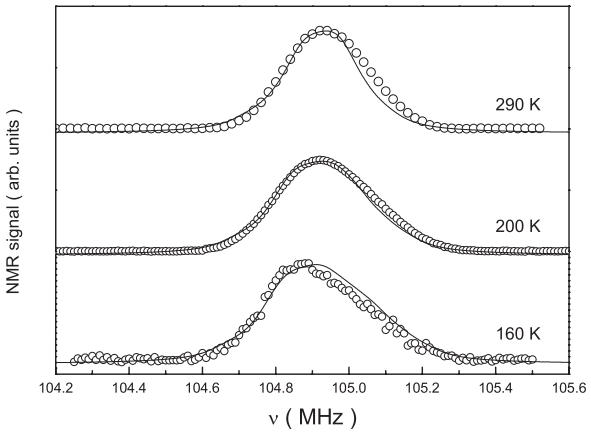

Figure 13. A comparison between experimental (circles) and theoretical (lines) powder ^{7}Li NMR spectra for $LiMnPO_4$. The calculated spectra were obtained by using equations (8)–(14).

to take the time averaged value of the electronic spin. The time averaged value of the electron spin is proportional to the molar susceptibility $\chi_{\rm mol}$:

$$N_{\rm a}\mu_0\mu_{\rm B}g\langle\vec{S}\rangle = \chi_{\rm mol}\vec{B}. \tag{11}$$

In the second term the sum goes over all neighbouring moments M and tensor $\mathbf{T}^k$ is the dipolar coupling tensor, which is traceless as long as the g-factor is isotropic. The dipolar tensor is, in the electron–nuclear point dipole approximation, given by [26]

$$\mathbf{T} = \frac{\mu_0}{4\pi}g\mu_{\rm B}\gamma_n\sum_k\frac{3\hat{n}_k\otimes\hat{n}_k - \mathbf{1}}{r_k^3}. \tag{12}$$

Here $\hat{n}_k$ is the unit vector denoting the direction cosines of the electron–nuclear $\vec{r}_k$ in the crystal frame. The sum goes over all k magnetic moments M. We have used the structural data and calculated the dipolar sum for a given Li site. The components of the tensor $\mathbf{T}$ are, for the $LiMnPO_4$ structure, then given by

$$\mathbf{T} = \frac{\mu_0}{4\pi}g\mu_{\rm B}\gamma\begin{pmatrix} 0.270 & -0.018 & 0.025 \\ -0.018 & -0.109 & 0.014 \\ 0.025 & 0.014 & -0.161 \end{pmatrix}[10^{30}\ {\rm m}^{-3}]. \tag{13}$$

The last term is due to the quadrupole interaction $\mathcal{H}_{\rm Q}$. In the principle axis system this interaction can be written as

$$\mathcal{H}_{\rm Q} = \frac{e^2qQ}{4I(2I-1)}\left(3I_z^2 - I(I+1) + \frac{1}{2}\eta(I_+^2 + I_-^2)\right) \tag{14}$$

where e^2qQ is the quadrupole frequency and η is the asymmetry parameter.

In figure 13 we compare the experimental and theoretical powder ^{7}Li NMR spectra for $LiMnPO_4$ in the paramagnetic phase. Here the only free fitting parameter was e^2qQ. The temperature evolution of the spectra, including the broadening of the line, is hidden in the temperature dependence of the spin susceptibility $\chi_{\rm mol}$, which was taken from the SQUID data. The agreement is rather good over the entire temperature range. We stress that we could also fit the powder ^{7}Li NMR spectra for $LiFePO_4$ in the same way, except for the different T_2 value (i.e. broadening of the spectra).

The experimental spectra could be fitted even below $T_{\rm N}$. However, here the two samples differ qualitatively. For $LiFePO_4$ the NMR linewidth becomes smaller suggesting that the

averaged value of the electronic spin 'seen' by the ^{7}Li nuclei becomes smaller, as expected for the antiferromagnetically ordered sample. On the other hand, for $LiMnPO_4$ the spectra dramatically broaden below T_N, suggesting an increase of the local magnetic field. It seems that on this point the magnetization measurements and ^{7}Li NMR measurements completely agree. Such a broadening could be due to the canting of the magnetic moments leading to a weak ferromagnetism. In such a case the canting angle must be very small, of the order of 0.1°. The other possibility is connected to the presence of some oxygen vacancies, which could change the Mn valence state and lead to ordered 'uncompensated' magnetic moments. We should however then observe a multi-component NMR spectrum, which is obviously not the case here. The presence of oxygen vacancies alone is thus not enough to account for the broadening of the entire ^{7}Li NMR line for $LiMnPO_4$. However, such oxygen vacancies could act as a pinning centre for soliton excitations, as suggested by the EPR measurements discussed earlier. In this case the effect of oxygen vacancies could be much more far reaching and could be easily seen also in the ^{7}Li NMR spectra as a dramatic broadening of the line. This could also explain the fact that the soliton energy obtained is 144 K and is about 20% smaller than the theoretical value calculated from equation (7) [22].

NMR relaxation times are important parameters in the understanding of phase transitions as they contain direct information about the fluctuations of the electronic spins. We will use the classical Kubo–Tomita–Moriya approach [27, 28]. Within this model the nuclear spin–lattice relaxation time is given by

$$T_1^{-1} = \sum_{\alpha 0 \leqslant q \leqslant \pi} |K_\alpha(q)|^2 S_\alpha(q, \omega_N) n_\alpha(q), \tag{15}$$

where $K_\alpha(q)$ is the electron–nuclear coupling described earlier, $S_\alpha(q, \omega_N)$ is the dynamic structure factor of the magnetic excitations, ω_N is the nuclear resonance frequency and $n_\alpha(q)$ is the corresponding occupation function. At high temperatures, where $\hbar\omega_N \ll k_B T$, this expression reduces to

$$T_1^{-1} = \gamma_N^2 k_B T \sum_{q,\alpha} |K_\alpha(q)|^2 \frac{\chi''_\alpha(q, \omega_N)}{\omega_N}. \tag{16}$$

We mention that the spin–spin lattice relaxation time T_2 of the ^{7}Li NMR line is also given by the same dynamic structure factor, but this time at $\omega = 0$:

$$\delta\nu \propto \frac{1}{T_2} \propto \sum_{\vec{q}} K_\alpha(\vec{q}) S_\alpha(\vec{q}, 0). \tag{17}$$

Now, if we assume that the dissipative part of the dynamic spin susceptibility $\chi''_\alpha(q, \omega_N)$ is simply proportional to the static magnetic susceptibility measured by the SQUID or from the first moment of the line, we can indeed successfully describe the temperature dependence of T_1 in the paramagnetic phase. Using similar arguments one can also explain the temperature dependence of T_2 shown in figure 11.

In the vicinity of a phase transition, however, it is the dynamic structure factor $S_\alpha(q, \omega)$ which determines the temperature dependence of T_1. When the critical fluctuations become enhanced due to the divergence of the spin correlation length near T_N, then one has $S_\alpha(q, \omega) \propto (T/T_N - 1)^{-\beta}$ and the relaxation times should show a tendency for divergent behaviour. This has indeed been observed. However, below T_N one may assume that n_α is the limiting factor for the relaxation. If n_α is determined by the soliton density, then one expects to observe a strong increase of relaxation times (or decrease of the relaxation rates), as has been observed. The relaxation data thus seem to support the physical picture of pinned solitons obtained from the EPR linewidth data. The fact that the stretched exponential parameter α is smaller for our $LiMnPO_4$ sample also suggests that the concentration of pinning sites is rather higher in this sample than in the bulk samples and may thus be responsible for the occurrence of weak ferromagnetism.

5. Conclusions

In conclusion, we have compared the magnetic properties of $LiMnPO_4$ and $LiFePO_4$ powders as prepared for electrochemical applications. Interestingly, we found that the magnetic ground state of $LiMnPO_4$ is very sensitive to various crystal imperfections and readily changes from the collinear antiferromagnetic state to a weak ferromagnetic state. This is not the case for $LiFePO_4$, whose collinear antiferromagnetic ground state is very robust. We suggest that solitons may be very important magnetic excitations in this system and that pinning of solitons below T_N together with frustration may play a decisive role in the formation of a weak ferromagnetic state in $LiMnPO_4$. The difference in stability of the magnetic ground states clearly reflects the difference in electronic structure of the two compounds and should be taken into account in further electrochemical studies. In the light of these results it would be interesting to investigate the variation of the electrochemical and magnetic properties as a function of the particle size, morphology and sample preparation conditions.

Acknowledgments

AD acknowledges the financial support of NATO (grant number SfP 976913) and the EU through the ALCANDO project, contract No G5MA-CT-2002-04023.

References

[1] Padhi A K, Nanjundaswamy K S and Goodenough J B 1997 *J. Electrochem. Soc.* **144** 1188
[2] Huang H, Yin S-C and Nazar L F 2001 *Electrochem. Solid-State Lett.* **4** A170
[3] Yamada A and Chung S-C 2001 *J. Electrochem. Soc.* **148** A960
[4] Li G, Azuma H and Tohda M 2002 *Electrochem. Solid-State Lett.* **5** A135
[5] Delacourt C, Poizot P, Morcrette M, Tarascon J-M and Masquelier C 2004 *Chem. Mater.* **16** 93
[6] Arčon D, Zorko A, Cevc P, Dominko R, Bele M, Jamnik J, Jagličič Z and Golosovsky I 2004 *J. Phys. Chem. Solids* at press
[7] Santoro R P, Segal D J and Newman R E 1966 *J. Phys. Chem. Solids* **27** 1192
[8] Mays J M 1963 *Phys. Rev.* **131** 38
[9] Goni A, Lezama L, Barberies G E, Pizzaro J L, Arriortua M I and Rojo T 1996 *J. Magn. Magn. Mater.* **164** 251
[10] Santoro R P and Newman R E 1967 *Acta Crystallogr.* **22** 344
[11] Rousse G, Rodriguez-Carvajal J, Patoux S and Masquelier C 2003 *Chem. Mater.* **15** 4082
[12] Bozorth R M and Kramer V 1959 *J. Phys. Rad.* **20** 393
[13] Gaberščček M, Dominko R, Bele M, Remškar M, Hanžel D and Jamnik J 2004 submitted
[14] Dominko R, Gaberščček M, Bele M, Remškar M, Hanžel D and Jamnik J 2003 *LiBD Electrode Materials (Sept. 2003)* (Extended Abstracts, Abstract No. 8)
[15] Gaberščček M, Bele M, Drofenik J, Dominko R and Pejovnik S 2001 *Electrochem. Solid-State Lett.* **4** A187
[16] Zaspel C E, Grigereit T E and Drumheller J E 1995 *Phys. Rev. Lett.* **74** 4539
[17] Curely J and Rouch J 1998 *Physica* B **254** 298
[18] Richards P M 1976 *Local Properties at Phase Transitions* ed K A Müller (Amsterdam: North-Holland) p 539
[19] Soos Z G, Cheung T T P and McGregor K T 1977 *Chem. Phys. Lett.* **46** 600
[20] Seehra M S and Castner T C 1968 *Phys. Kondens. Mater.* **7** 185
[21] Belavin A A and Polyakov A M 1975 *JETP Lett.* **22** 245
[22] Subbaraman K, Zaspel C E and Drumheller J E 1998 *Phys. Rev. Lett.* **80** 2201
[23] Tucker M C, Doeff M M, Richardson T J, Finones R, Cairns E J and Reimer J A 2002 *J. Am. Chem. Soc.* **124** 3832
[24] Slichter C P 1992 *Principles of Magnetic Resonance* (New York: Springer)
[25] Ganguly P, Venkatraman T N, Pradhan S, Rajamohanan P and Ganapathy S 1996 *J. Phys. Chem.* **100** 5017
[26] Schweiger A and Jeschke G 2001 *Principles of Pulsed Electron Paramagnetic Resonance* (Oxford: Oxford University Press)
[27] Kubo R and Tomita K 1954 *J. Phys. Soc. Japan* **9** 888
[28] Moriya T 1962 *Prog. Theor. Phys.* **28** 371